



1     **Investigating the relationship between volume**  
2     **transport and sea surface height in a numerical**  
3     **ocean model**

4     Estee Vermeulen <sup>1,2\*</sup>, Björn Backeberg <sup>2,3,4</sup>, Juliet Hermes <sup>1,5</sup>, Shane Elipot <sup>6</sup>

5     <sup>1</sup> *Department of Oceanography, University of Cape Town, Rondebosch, South Africa*

6     <sup>2</sup> *Nansen-Tutu Centre for Marine Environmental Research, University of Cape Town, South*  
7     *Africa*

8     <sup>3</sup> *CSIR, Coastal Systems Research Group, Stellenbosch, South Africa*

9     <sup>4</sup> *Nansen Environmental and Remote Sensing Centre, Bergen, Norway*

10    <sup>5</sup> *South African Environmental Observation Network, Egagasini Node, Cape Town, South*  
11    *Africa*

12    <sup>6</sup> *Rosenstiel School of Marine and Atmospheric Science, University of Miami, 4600*  
13    *Rickenbacker Causeway, Miami, FL 33149*

14    \* *Corresponding author address:* Estee Vermeulen, Department of Oceanography, University of  
15    Cape Town, Rondebosch, South Africa

16    Email: [esteever01@gmail.com](mailto:esteever01@gmail.com)



## 17 Abstract

18 The Agulhas Current Time-series mooring array (ACT) measured transport of the Agulhas  
19 Current at 34°S for a period of 3 years. Using along-track satellite altimetry data directly  
20 above the array, a proxy of Agulhas Current transport was developed based on the relationship  
21 between cross-current sea surface height (SSH) gradients and the measured transports. In this  
22 study, the robustness of the proxy is tested within a numerical modelling framework, using a  
23 34-year long regional-hindcast simulation from the Hybrid Coordinate Ocean Model (HYCOM).  
24 Two reference proxies were created using HYCOM data from 2010-2013, extracting model data  
25 at the mooring positions and along the satellite altimeter track for; (1) the box transport  
26 ( $T_{\text{box}}$ ) and (2) the jet (southwestward) transport ( $T_{\text{jet}}$ ). Next, sensitivity tests were performed  
27 where the proxy was recalculated from HYCOM for (1) a period where the modelled vertical  
28 stratification was different compared to the reference proxy, and (2) different lengths of periods:  
29 1, 3, 6, 12, 18 and 34 years. Compared to the simulated (native) transports, it was found that  
30 the HYCOM proxy was more capable of estimating the box transport of the Agulhas Current  
31 compared to the jet transport. The HYCOM configuration in this study contained exaggerated  
32 levels of offshore variability in the form of frequently-impinging baroclinic anticyclonic eddies.  
33 These eddies consequently broke down the linear relationship between SSH slope and vertically-  
34 integrated transport, resulting in stronger correlations for the inshore linear regression models  
35 compared to the ones offshore. Vertically-integrated transport estimates were therefore more  
36 accurate inshore than those offshore or when the current was in a meandering state. Results  
37 showed that calculating the proxy over shorter or longer time periods in the model did not  
38 significantly impact the skill of the Agulhas transport proxy, suggesting that 3-years was a  
39 sufficiently long time-period for the observation based transport proxy.



## 40 1 Introduction

41 The Agulhas Current System is the strongest western boundary current in the Southern  
42 Hemisphere and transports warm tropical water southward along the east coast of South  
43 Africa [Lutjeharms, 2006]. The Agulhas Current, in the northern region, is known for  
44 its narrow, fast, flow conditions following the steep continental slope [de Ruijter et al.,  
45 1999]. As the current continues southwestward the current becomes increasingly unstable  
46 over the widening continental shelf until it eventually retroflects, forming an anticyclonic  
47 loop south of Africa and returning to the Indian Ocean as the eastward Agulhas Return  
48 Current [Beal et al., 2011; Biastoch and Krauss, 1999; Dijkstra and de Ruijter, 2001;  
49 Hermes et al., 2007; Lutjeharms, 2006; Loveday et al., 2014]. The anticyclonic loop, known  
50 as the Agulhas retroflection, contains some of the highest levels of mesoscale variability  
51 in the global ocean [Gordon, 2003] through the formation of Agulhas rings, eddies and  
52 filaments. This, in turn, contributes significantly to the Benguela upwelling system, the  
53 Atlantic Ocean and the global overturning circulation system [Gordon et al., 1987; Beal  
54 et al., 2011; Durgadoo et al., 2013], thereby impacting the Atlantic Meridional Overturning  
55 Circulation (AMOC) by providing a salt-advective feedback through a process known  
56 as the Agulhas leakage [Biastoch and Krauss, 1999; Beal et al., 2011; Durgadoo et al.,  
57 2013; Loveday et al., 2014]. In the regional context, the Agulhas Current has a major  
58 influence on the local weather systems, due to large latent and sensible heat fluxes, which  
59 contributes to rainfall and storm events over the adjacent land [Reason, 2001; Rouault  
60 et al., 2002; Rouault and Lutjeharms, 2003]. The unique circulation of the Agulhas  
61 Current System, in the context of regional and global climates, makes it an important  
62 field of research.

63 To understand the complicated dynamics of the Agulhas Current requires an integrated  
64 approach using numerical ocean models, satellite remote sensing measurements and *in situ*  
65 observations. Previous studies have suggested that measuring the dynamics of the Agulhas  
66 Current in the northern region is easier due to its stable trajectory and its confinement to  
67 the continental slope [van Sebille et al., 2010]. However, the close proximity of the current  
68 to the coast makes it difficult to monitor using satellite altimetry [Rouault et al., 2010].  
69 In addition, the frequent disturbances of the current in the form of solitary meanders, also



70 known as Natal Pulses, and its interactions with mesoscale features originating upstream  
71 and from the east [Elipot and Beal, 2015], remain poorly resolved in many numerical  
72 ocean models [Tsubawa and Hasumi, 2010; Braby et al., 2016], highlighting the challenges  
73 involved in monitoring and modelling the dynamics in this region.

74 There is a trade-off between spatial and temporal sampling. *In situ* observations may  
75 accurately measure the dynamics of the Agulhas Current throughout the water column  
76 but are expensive and spatially coarse. In contrast, satellite observations can provide  
77 high spatial resolution data of the surface ocean but lacks detailed information below  
78 the surface. Hence, numerical models are needed to provide a temporally coherent, high  
79 resolution representation of the ocean throughout the water column. Numerous studies  
80 aiming to monitor long-term changes in global current systems have adopted methods  
81 to combine various sampling tools [eg. Maul et al. 1990; Imawaki et al. 2001; Andres  
82 et al. 2008; Zhu et al. 2004; Yan and Sun 2015], including the recent development of the  
83 Agulhas transport proxy established to monitor the interannual variability and long-term  
84 trends in Agulhas Current transport [Beal and Elipot, 2016].

85 The Agulhas transport proxy of Beal and Elipot [2016] was derived from the physical  
86 principle of geostrophy, where along-track sea surface height slope measured by satellite  
87 altimeters can ultimately be related to a measure of volume transport across a portion  
88 of the current, provided that the surface current represents the flow at depth [Beal and  
89 Elipot, 2016]. Beal and Elipot [2016] have shown that a strong relationship exists between  
90 surface geostrophic velocity and full-depth transport such that sea level anomalies can  
91 be used to study the variability and dynamics of the Agulhas Current System as has  
92 been demonstrated before [Fu et al., 2010; Rouault et al., 2010; Rouault and Penven,  
93 2011; etc.]. The 22-year transport proxy created by Beal and Elipot [2016] assumed  
94 a fixed linear relationship between *in situ* transport and sea surface slope based on *in*  
95 *situ* measurements over the 3-year sampling period of the Agulhas Current Time-series  
96 experiment (ACT) [Beal et al., 2015]. Analyses of the Agulhas Current transport proxy  
97 time-series concluded that the Agulhas Current has not intensified over the last two  
98 decades in response to intensified global winds under anthropogenic climate change [Cai,  
99 2006; Yang et al., 2016], but instead has broadened as a result of increased eddy activity  
100 [Beal and Elipot, 2016] in agreement with Backeberg et al. [2012].



101 This modelling study aimed to recreate the Agulhas transport proxy developed by Beal  
102 and Elipot [2016], within a regional HYCOM simulation of the greater Agulhas Current  
103 System in order to test the validity of the underlying assumptions on which the satellite-  
104 altimeter derived proxy was based. Firstly, the Agulhas Current transport proxy was  
105 recreated using modelled data from HYCOM following the methodology of Beal et al.  
106 [2015] and [Beal and Elipot, 2016] for the data period 2010-2013. This reference proxy  
107 allowed for the relationship between Agulhas Current transports and sea surface slope  
108 across the Agulhas Current Time-series experiment (ACT) array to be investigated in  
109 HYCOM. Following this, the impact of the vertical variability of the current on the accu-  
110 racy of the transport proxy was assessed. Finally, the optimal length scale of observations  
111 needed to build a strong linear relationship between transport and SSH slope was tested  
112 by recalculating the proxy using 1, 3, 6, 12, 18 and 34 years of HYCOM data.

113 Assuming a constant vertical stratification over the 3-year sampling period, and hence  
114 ignoring baroclinic changes that could potentially impact the linear relationship between  
115 sea surface slope and full-depth transport could become problematic when generating a  
116 22-year proxy of Agulhas Current transports. Therefore, key questions for this paper in-  
117 clude: (1) How is the linear relationship between transport and sea surface slope affected  
118 when recalculating the proxy over longer time-periods in HYCOM? (2) How will changes  
119 in the vertical structure of the Agulhas Current impact the transport proxy? Theoret-  
120 ically the vertical velocity structure changes during mesoscale meander events Zhu et al.  
121 [2004] and thermohaline processes [Beal and Elipot, 2016] since horizontal changes in  
122 stratification result in changes in the velocity structure with depth. Perhaps even changes  
123 in the strength of the Agulhas Undercurrent may impact the transport proxy. Finally,  
124 (3) what would be the ideal sampling period needed to build a strong, linear relationship  
125 between transport and SSH slope? Building the linear relationship over periods longer  
126 than 3 years could perhaps increase the skill of the transport proxy by averaging out  
127 random perturbations, but may be also be affected by the interannual variability of the  
128 current system [Elipot and Beal, 2018]. This study aims to test the robustness of using 3  
129 years of *in situ* mooring data to develop a satellite altimetry derived transport proxy for  
130 the Agulhas Current at 34°S, by testing the underlying assumptions in a numerical mod-  
131 elling framework. This can assist in planning future deployments of moorings ultimately



132 facilitating the improvement of an integrated ocean observing system for the Agulhas  
133 Current.

134 This paper is structured as follows; Section 2 describes the data and methods, it should  
135 be noted that this section forms a key part of the paper as the methods of recreating the  
136 proxy are an integral component of the study. Section 3 presents the results from the  
137 HYCOM transport proxy and lastly Section 4 presents the summary and conclusions.

## 138 2 Data and Methods

### 139 2.1 The Hybrid Coordinate Ocean Model

140 The Hybrid Coordinate Ocean Model (HYCOM) is a primitive equation ocean model  
141 that was developed from the Miami Isopycnic Coordinate Ocean Model (MICOM) [Smith  
142 et al., 1990]. HYCOM combines the optimal features of isopycnic-coordinate and fixed-  
143 grid ocean circulation models into one framework [Bleck, 2002] and uses the hybrid layers  
144 to change the vertical coordinates depending on the stratification of the water column.  
145 The model makes a dynamically smooth transition between the vertical coordinate types  
146 via the continuity equation using the hybrid coordinate generator [Chassignet et al., 2007].  
147 Well-mixed surface layers use z-level coordinates,  $\rho$ -coordinates are utilized between the  
148 surface and bottom layers in a well-stratified ocean, and the bottom layers apply  $\sigma$ -  
149 coordinates following bottom topography. Adjusting the vertical spacing between the  
150 hybrid coordinate layers in HYCOM simplifies the numerical implementation of several  
151 physical processes without affecting the efficient vertical resolution, and in doing so com-  
152 bines the advantages of the different coordinate types in optimally simulating coastal and  
153 open-ocean circulation features [Chassignet et al., 2007].

154 The HYCOM output in this study was made available from a nested  $1/10^\circ$  model of  
155 the greater Agulhas Current System (AGULHAS) [Backeberg et al., 2008; 2009; 2014].  
156 The regional nested model, AGULHAS, received boundary conditions from the basin-  
157 scale model of the Indian and Southern Ocean (INDIA) [George et al., 2010] every 6-hrs.  
158 The boundary conditions were relaxed towards the outer model over a 20 grid cell buffer  
159 zone. The horizontal resolution of the parent model ranged from 14 km in the northern  
160 Indian Ocean to 45 km in the Southern Ocean, with a resolution ranging from 30 to 40



161 km in the region of the Agulhas Current. The nested model covered the region from  
162 the Mozambique Channel to the Agulhas Retroflexion region and the Agulhas Return  
163 Current, geographically extending from approximately 0°-60° East and from 10°-50° South,  
164 with a horizontal resolution of ~10 km that adequately resolved mesoscale dynamics to  
165 the order of the first baroclinic Rossby radius estimated to be about 30 km [Chelton et al.,  
166 1998]. Both models have 30 hybrid layers and targeted densities ranging from 23.6 to 27.6  
167 kg/m<sup>3</sup>.

168 The parent model was initialised from Levitus climatology (WOA05) [Antonov and Levi-  
169 tus, 2006] and spun up for 10 years using climatological ERA-interim forcing [Dee et al.,  
170 2011]. AGULHAS was initialised from a balanced field of the parent model interpolated  
171 to the high-resolution grid. Both models were then run from 1980 to 2014 using inter-  
172 annual forcing from ERA40 [Uppala et al., 2005] and ERA-interim [Dee et al., 2011].  
173 Version 2.2 of the HYCOM source code has been used in this model and, together with  
174 the second order advection scheme, provides an adequate representation of the Agulhas  
175 Current [Backeberg et al., 2014]. However, limitations of the free running model include  
176 high levels of SSH variability south of Madagascar and offshore of the Agulhas Current,  
177 suggesting that eddy trajectories may be too regular in the model [Backeberg et al.,  
178 2014]. The data available for this study was a weekly output of the regional HYCOM  
179 model of the Agulhas region from 1980 to 2014. See table 1 for a summary of the model  
180 configuration.

## 181 2.2 The Agulhas Current Time-series Experiment

182 The ACT experiment was established to notably obtain a multi-decadal proxy of Agulhas  
183 Current transport using satellite altimeter data. The first phase of the experiment was  
184 the *in situ* phase where the ACT mooring array was deployed in the Agulhas Current,  
185 near 34°S, for a period of three years from 2010-2013 [Beal et al., 2015]. The second  
186 phase was the development of the transport proxy, where sea surface height along the  
187 ACT section, obtained from along-track satellite altimetry, was regressed to the *in situ*  
188 transport measurements [van Sebille et al., 2010; Beal and Elipot, 2016]. To optimally fa-  
189 cilitate the regression between the transport and altimetry, the ACT array was collocated  
190 with the altimeter track number 96 successively occupied by satellites TOPEX/Poseidon



Table 1: HYCOM specifications.

<b>Model</b>	HYCOM (regional)
<b>Configuration</b>	AGULHAS (nested)
<b>Nested domain</b>	0°-60°E; 10°-50°S
<b>Time period</b>	1980-2014
<b>Resolution</b>	1/10°; Weekly (7/8 days)
<b>Grid spacing (km)</b>	~10 km
<b>Vertical discretization</b>	30 hybrid layers Target densities (+1,000 kg/m <sup>3</sup> ) layer 1 - layer 30: 22.30, 22.60, 22.90, 23.20, 23.50, 23.80, 24.10, 24.40, 24.70, 25.00, 25.30, 25.60, 25.90, 26.20, 26.50, 26.80, 26.89, 26.99, 27.08, 27.18, 27.27, 27.37, 27.46, 27.56, 27.65, 27.75, 27.84, 27.94, 28.00, 28.05
<b>Bathymetry</b>	GEBCO 1'
<b>Atmospheric forcing</b>	6-hourly ERA-interim reanalysis data (1/4°) resolution
<b>Boundary forcing</b>	Parent model (INDIA)
<b>Advection scheme</b>	2 <sup>nd</sup> order
<b>Vertical mixing scheme</b>	KPP

191 (1992-2002), Jason-1 (2002-2008) and currently Jason-2 (since 2008) and Jason-3 (since  
 192 2016) [Beal and Elipot, 2016] (Figure 1).

193 During the first phase of the ACT experiment, the mooring array was maintained in the  
 194 Agulhas Current for a period of 34 months, perpendicular to the continental slope at  
 195 34°S, south of East London, South Africa (Figure 1). The array was made up of 12 sites;  
 196 site A through G were full-depth current meter moorings which were, on average, 26 km  
 197 apart. Sites P2-P5 were CPIES (Current- and Pressure-recording Inverted Echo Sounders)  
 198 placed 50 km apart. The CPIES were used to estimate the geostrophic cross-track velocity  
 199 beyond mooring G so that the Agulhas Current variability was fully-captured during

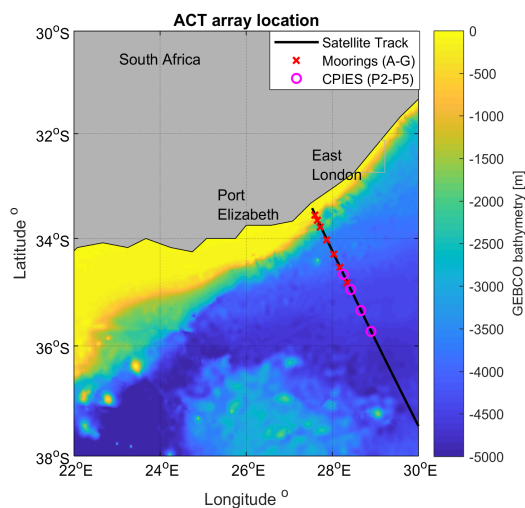


Figure 1: Geographical location of the ACT array with the mooring (red crosses) and CRIES (magenta circles) stations relative to the T/P, Jason-1,2,3 satellite track #96 (black line). Colour shading illustrates the GEBCO bathymetry (m).

200 meander events [Beal et al., 2015]. From the data collected in Beal et al. [2015], two  
 201 volume transports were estimated: (1) a box or boundary layer transport ( $T_{box}$ ) and (2)  
 202 a western boundary jet transport ( $T_{jet}$ ).  $T_{box}$  is a net transport within a fixed distance  
 203 from the coast, while  $T_{jet}$  is a stream dependent transport that is calculated by changing  
 204 the boundaries of integration at each time step depending on the strength and cross-  
 205 sectional area of the southwestward jet. The western boundary jet transport algorithm  
 206 was developed to specifically exclude the northeastward transport during meander events,  
 207 occurring inshore of the meander [Beal et al., 2015].

208 During the second phase of the ACT experiment, Beal and Elipot [2016] built a 22-year  
 209 transport proxy by regressing the three years of *in situ* transport measurements against  
 210 along-track satellite altimeter data spanning the years 1993-2015. Beal and Elipot [2016]  
 211 noted the importance of the relationship between sea surface height and transport when  
 212 inferring trends in the current structure based on satellite altimetry and remained cautious  
 213 regarding the assumptions used to validate the proxy. In order to obtain transport estim-  
 214 ates using altimetry, it was also important to define accurate boundaries for the Agulhas  
 215 Current to distinguish whether the current is stable or meandering and to determine the  
 216 width of the current to calculate  $T_{box}$  and  $T_{jet}$ .



## 217 2.3 Development of the Agulhas transport proxy

218 Based on physical principles sea surface slope is proportional to surface geostrophic velo-  
219 city. Previous analyses have shown that the vertical structure of the Agulhas Current is  
220 barotropic [Elipot and Beal, 2015], such that the direction of current velocity anomalies  
221 does not change significantly with depth. This suggests that the relationship between sur-  
222 face geostrophic velocity and full depth transport should be strong, despite the presence of  
223 the Agulhas Undercurrent [Beal and Elipot, 2016]. The relationship between sea surface  
224 slope and transport was therefore tested using linear regression models, which explicitly  
225 described a relationship between the predictor variable, sea surface slope and the response  
226 variable, transport per unit distance [van Sebille et al., 2010; Beal and Elipot, 2016].

227 The transport proxy created by Beal and Elipot [2016] was initially developed by finding a  
228 linear relationship between transport and sea surface slope across the entire length of the  
229 ACT array, a common method used in previous studies [Imawaki et al., 2001; van Sebille  
230 et al., 2010; Sprintall and Revelard, 2014; Yan and Sun, 2015]. However, this method lead  
231 to uncertainty in the linear regression due to the strong, co-varying sea surface height  
232 across the current. The preferred method was therefore to build nine individual linear  
233 regression models, one for each mooring position and CPIES-pairs along the ACT array,  
234 which locally related transport to sea surface slope [Beal and Elipot, 2016]. It is important  
235 to note that the regression models assumed a constant, linear relationship between sea  
236 surface slope and transport over the three-year *in situ* period. The transport variable in  
237 the regression models was defined as transport per unit distance ( $T_x$  and  $T_{xsw}$ ), i.e. the  
238 vertically integrated velocity with units in  $\text{m}^2\text{s}^{-1}$ . The total transports,  $T_{box}$  and  $T_{jet}$   
239 in  $\text{m}^3\text{s}^{-1}$ , were calculated by integrating the  $T_x$  and  $T_{xsw}$  estimates, predicted from the  
240 regression models, to the respective current boundaries.

## 241 2.4 Recreating the Agulhas transport proxy in HYCOM

### 242 2.4.1 Model Transport

243 In order to recreate the Agulhas Current proxy in HYCOM, data corresponding to the  
244 measurements collected from the ACT mooring array were extracted from the model.



245 The barotropic velocity -equivalent to an integral of the velocity with depth- from each  
246 mooring location (A-G) and CPIES pairs P3-P4 and P4-P5 was extracted for the 34-year  
247 model period. Extracting the barotropic velocity component from each mooring avoided  
248 interpolation errors that may have occurred if the model velocity was interpolated onto  
249 the locations of each current-meter instrument on each mooring [e.g. van Sebille et al.,  
250 2010]. Transport per unit distance ( $T_x$ ) for each mooring was calculated by multiplying  
251 the cross-track barotropic velocity by the respective depth at each mooring location and  
252 the sea surface slope for each of the locations were obtained from the model (see next  
253 section) (hereafter CPIES pairs P3-P4 and P4-P5 were included as mooring positions 8  
254 and 9). The same method was employed to build regression models between sea surface  
255 slope and the southwestward component of the flow ( $T_{xsw}$ ), as is required to ultimately  
256 calculate the jet transport ( $T_{jet}$ ) [Beal et al., 2015].

257 To assess the accuracy of the transport proxy, the HYCOM transport proxy was compared  
258 to the simulated (native) transport in HYCOM to quantify the differences between the  
259 proxy and modelled transports and hence understand which processes the proxy may fail  
260 to represent. The transport across the ACT section in HYCOM was extracted by setting  
261 up the grid points between the two coordinates defining the start and end of the section  
262 following the great circles of the sphere and calculating the defined transport at each  
263 grid point along the section. The transport calculation facilitated a separation of the  
264 transports into two components: the box transport ( $T_{box}$ ) and the jet transport ( $T_{jet}$ ).

#### 265 2.4.2 Model SSH

266 In order to reproduce the “along-track” SSH altimeter data needed to create the proxy as  
267 in Beal and Elipot [2016], 34 years of HYCOM SSH was linearly interpolated onto the  
268 coordinates of the TOPEX/Jason satellite track number 96 overlapping the model ACT  
269 array. The coordinates of the along-track altimeter data were obtained from the filtered 12  
270 km Jason-2 Aviso satellite product, and not the unfiltered 6 km product which was used  
271 for the original ACT proxy [Beal and Elipot, 2016], since the 12 km product matched the  
272 ~10 km model resolution more closely. To obtain the sea surface slope for each regression  
273 model, an optimal pair of SSH data points was chosen such that the horizontal length



274 scale between them allowed for a maximum correlation between the sea surface slope  
275 and  $T_x$ . The length scales of the slopes ranged from 24 km at mooring A to 12 km at  
276 mooring G and 48 km for the offshore CPIES-pairs, indicating an increase in the spatial  
277 scale of offshore flow, possibly due to increased offshore variability. Results from the *in*  
278 *situ* proxy experiment by Beal and Elipot [2016] also showed an increasing length scale  
279 with increasing distance offshore, however the results varied considerably in magnitude:  
280 27 km at mooring B to 102 km at mooring G. In this study the SSH slope was calculated  
281 such that a negative SSH slope corresponds to a negative surface velocity (southwest)  
282 according to geostrophy, whereas a positive slope would indicate positive northeastward  
283 flow.

#### 284 **2.4.3 Building the regression models**

285 Nine linear regression models were first developed to estimate the transport per unit  
286 distance ( $T_x$  and  $T_{xsw}$ ) from the HYCOM sea surface slope during approximately the  
287 same three-year period over which the ACT proxy was developed (April 2010- February  
288 2013). The three-year time period will further be referred to as the reference period.  
289 Further tests were later performed, where the proxy was calculated over a range of different  
290 time periods (see section 2.6).

291 To calculate the total transport across the ACT array requires continuous  $T_x$  estimates  
292 across the current. This was achieved as in Beal and Elipot [2016] by fitting a piece-  
293 wise cubic Hermite interpolating polynomial function to obtain transport estimates at 1  
294 km intervals from the coast to the end of the array (Figure 2). Fitting the transport  
295 function to the coast and equating it to zero would be equivalent to implementing a no  
296 slip boundary condition in the model. Before calculating the total transport the current  
297 boundaries needed to be defined. The box transport ( $T_{\text{box}}$ ) was calculated by integrating  
298  $T_x$  horizontally to 230 km offshore, the three-year mean width of the current in HYCOM.  
299 The jet transport ( $T_{\text{jet}}$ ) was calculated using the algorithm developed by Beal et al., 2015  
300 by integrating  $T_{xsw}$ , the southwest transport component, to the first maximum of  $T_x$   
301 beyond the half-width of the current (115 km in HYCOM) at each time step (Figure 2).  
302 Beal et al. [2015] argued that  $T_{\text{jet}}$  therefore captured the southwestward transport of the

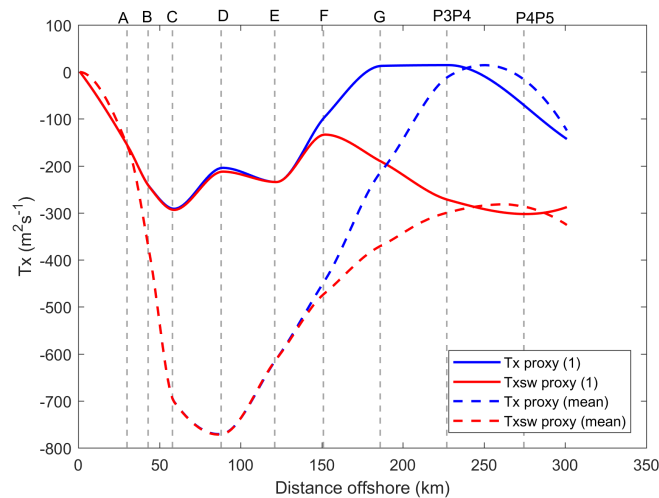


Figure 2: HYCOM transport per unit distance proxy ( $\text{m}^2 \text{s}^{-1}$ ) for  $T_x$  (blue) and  $T_{xsw}$  (red) transport at 1 km intervals at the first model time step (solid lines) and for the mean reference period (dashed lines). The faint grey lines represent the positions of moorings and offshore CPIES pairs.

303 meandering Agulhas Current.  $T_x$  and  $T_{xsw}$  are simply shown at the first model time step  
 304 (week of the 3<sup>rd</sup> of January 1980) in HYCOM and for the mean of the reference period  
 305 (2010-2013) to show the difference between the net and southwest transport components  
 306 used to calculate  $T_{box}$  and  $T_{jet}$  (Figure 2).

307 In order to test the accuracy of the transport proxy, it was first compared to the HYCOM  
 308 transport for the same period over which the proxy was developed (2010-2013). By  
 309 studying the corresponding model fields we were able to identify dynamic features in the  
 310 model that the proxy failed to capture. The correlation for the overlapping transports from  
 311 the model and the model proxy was calculated as well as the 3-year mean and standard  
 312 deviation (Table 3). Then, assuming that the three-year linear relationship between SSH  
 313 slope and transport per unit distance ( $T_x$  and  $T_{xsw}$ ) from 2010-2013 remains constant,  
 314 the regression models were applied to the entire 34-year SSH model data. This resulted  
 315 in transport per unit distance estimates ( $T_x$  and  $T_{xsw}$ ) for each mooring position at  
 316 each time step from 1980 to 2014. Thereafter, the 34-year transports were calculated by  
 317 applying the same methods that were used to calculate the 3-year transport time-series;  
 318 firstly, obtaining  $T_x$  estimates at 1 km-intervals along the array and secondly integrating



319 horizontally to obtain  $T_{box}$  and  $T_{jet}$  (Figure 2).

## 320 **2.5 Comparison of the transport proxy to actual model transports**

321 The simulated model transports were calculated using the full-depth velocity fields across  
322 the array. If the relationship between SSH slope and transport is strong, there would  
323 be good agreement between the proxy and the actual model transports. To quantify  
324 this correlations and transport statistics for the model and proxy were calculated from  
325 the two-time series. These provided insight into which processes the proxy may have  
326 failed to capture, which were then further investigated in HYCOM. Statistics are deemed  
327 significant at the 95% significance level.

328 Eddy kinetic energy (EKE) was calculated to show the surface variability of the current  
329 coincident with averaged SSH contours used to represent the mean surface structure  
330 (Figure 5). The eddy kinetic energy was calculated as follows:

$$EKE = \frac{(u')^2 + (v')^2}{2} \quad (1)$$

331 where  $u'$  and  $v'$  are the zonal and meridional geostrophic current anomalies relative to the  
332 geostrophic current mean calculated over the 3-year mean reference period, and over the  
333 highest and lowest correlated years. In order to evaluate the subsurface current structure  
334 along the ACT array, vertical velocity profiles were analysed for each mooring and CPIES-  
335 pair over the 3-year mean reference period as well as over the highest and lowest correlated  
336 years.

337 Transport variability in the HYCOM model was analysed by investigating residual trans-  
338 port events in the worst and best performing regression models. In order to examine  
339 the impacts of variable mesoscale features, residual transport events were identified as the  
340 outlying residual transport values above and below 2 standard deviations of the estimated  
341 transport.

$$e = Y_i - \hat{Y}_i \quad (2)$$

342 where  $e$  is the estimated residuals,  $Y_i$  is the HYCOM transport per unit distance value  
343 ( $Tx$ ) and  $\hat{Y}_i$  is the estimated transport per unit distance value according to the linear  
344 regression models.



345 To investigate the current structure during these residual events, composite averages of  
346 the cross-track velocity structure were analysed. The cross-track velocity at each depth  
347 layer in HYCOM was extracted at 12 km intervals from 0 km to 400 km offshore, for the  
348 34-year model period. Although the ACT array only reached 300 km offshore, analysis of  
349 the current structure in HYCOM was extended further offshore. Previous analyses have  
350 shown increased levels of offshore variability in this HYCOM simulation [Backeberg et al.,  
351 2009; 2014], which therefore made it interesting to study the subsurface structure during  
352 the offshore current meanders and the influence these could have on the transport proxy.  
353 To further investigate the effect of the residual transport values on the box transport  
354 proxy, considering it performed better than the jet transport proxy (see section 3.2), all  
355 corresponding transport events exceeding plus or minus two standard deviations were  
356 removed from each linear regression model during development of the proxy, after which  
357 the  $T_{box}$  proxy was re-calculated as explained in section 2.4.3 and evaluated against the  
358 initial box transport proxy.

## 359 2.6 Sensitivity tests

360 To test the sensitivity of the time span of observations used to create the transport  
361 proxy, sensitivity experiments were performed to test how many years of virtual *in situ*  
362 observations are needed to create an accurate proxy to monitor the Agulhas Current  
363 transport. Using 34 years of model data the linear relationship could be tested over much  
364 longer or shorter periods.

365 Using the method described in section 2.4.3, regression models were built for 1, 6, 12, 18  
366 and 34 years. In addition, the models were calculated over two arbitrary 3-year periods,  
367 to test the influence that different current dynamics over different years could have on the  
368 development of the transport proxy. Lastly, the regression models were calculated over  
369 the maximum and minimum annual transport years in HYCOM, as well as during the  
370 years the HYCOM transport standard deviation was the largest and the smallest. Table 2  
371 shows the time range over which the sensitivity experiments were performed. The 3-year  
372 *in situ* period in the model corresponded to the actual time range over which the *in situ*  
373 experiment was conducted, April 2010- February 2013 [Beal et al., 2015].



Table 2: Sensitivity experiment time periods.

Time range (years)	Model dates
1	Jan 2011 - Dec 2011
3	Apr 2010 - Feb 2013
6	Jan 2009 - Dec 2014
12	Jan 2003 - Dec 2014
18	Jan 1997 - Dec 2014
34	Jan 1980 - Dec 2014
3*	Jan 1980 - Dec 1982; Jan 2000 - Dec 2002
Max (Min) HYCOM transport.	2003 (1982)
Max (Min) HYCOM transport STD.	2013 (1980)

3\* Corresponds to the two additional 3-year periods

### 374 3 Results

#### 375 3.1 HYCOM linear regression models

376 The coefficient of determination ( $R^2$ ) from the regression models showed how well the  
 377 linear relationship predicts the transport per unit distance estimates in HYCOM (Figure  
 378 3). The  $R^2$  statistics from the regression models ranged from 0.86 at mooring A (30  
 379 km offshore) to 0.49 at the last CPIES-pair P4P5 (275 km offshore) for  $T_x$  and 0.86  
 380 at mooring A to 0.37 at P4P5 for  $T_{xsw}$  (P values  $< 10^{-3}$ ). Results from the *in situ*  
 381 experiment showed an increase in the  $R^2$  statistics in the regression models ranging from  
 382 0.51 at mooring A and 0.81 for CPIES-pair P4P5 for  $T_x$  [Beal and Elipot, 2016], thus  
 383 showing that the regression models had poorer skill inshore during the *in situ* experiment,  
 384 whereas in HYCOM the regression models have poorer skill offshore. The results from  
 385 the  $T_{xsw}$  regression models in HYCOM showed similar results for the inshore mooring  
 386 locations (A, B, C, E) with slightly higher correlations for offshore moorings F, G and  
 387 CPIES-pair P3P4 but a lower correlation for D and the furthest CPIES-pair P4P5. This  
 388 shows that the  $T_{xsw}$  regression models explained more variance for moorings F, G and  
 389 P3P4 but less variance for D and P4P5 than the  $T_x$  regression models.

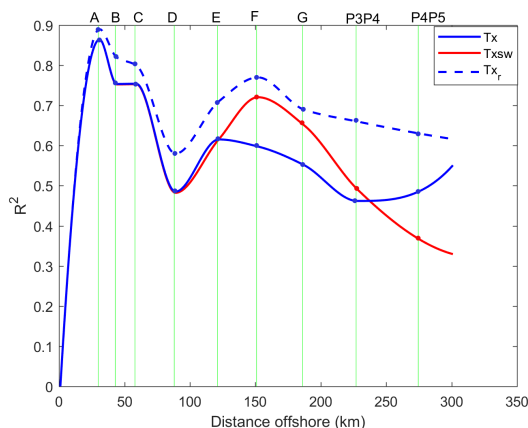


Figure 3:  $R^2$  statistics from the linear regression models showing the relationship between HYCOM SSH slope and HYCOM transport per unit distance for each mooring (A-G) and CPIES-pair (P3P4 & P4P5) over the 3-year reference period (2010-2013).  $T_x$  is represented by the solid blue line and  $T_{xsw}$  by the solid red line. The dashed blue line represents the results of  $T_x$  after the removal of the residual transport events (see section 3.4). Sites A - CPIES pair P4P5 are shown by the faint green lines.

### 390 3.2 Proxy validation

391 In order to test the accuracy of the box and jet HYCOM transport proxies, these were  
 392 compared to the box and jet transports extracted from HYCOM. This aided the invest-  
 393 igation in terms of identifying transport events or features the proxy failed to represent.

394 Based on the correlation of the 3-year proxy transport (2010-2013) to the model transport  
 395 over the same period, the box transport proxy explained 57% of the variance while the  
 396 jet transport proxy only explained 14% of the variance. Assuming a constant three-year  
 397 linear relationship for the nine regression models, the transport proxy was calculated using  
 398 34 years of HYCOM SSH slope, after which the 34-year box transport proxy explained  
 399 52% of the variance and the jet transport proxy explained 26% of the variance.

400 Table 3 summarises the transport statistics based on the 3-year and extended 34-year time  
 401 period. The 34-year mean transport and standard deviation from HYCOM for the box and  
 402 jet transport was  $-84 \pm 47$  Sv and  $-110 \pm 38$  Sv respectively. The proxy box transport  
 403 was  $-87 \pm 34$  Sv and the jet transport was  $-92 \pm 31$  Sv. A higher jet transport was  
 404 expected considering it excludes northeast counter-flows that decrease the box transport  
 405 [Beal et al., 2015]. The differences between the standard deviations between HYCOM and



Table 3: a) Summary of the transport statistics of the HYCOM model transport against the HYCOM proxy transport over the 3-year and extended 34-year time period. Negative values denote transport in the southwest direction.  $1 \text{ Sv} = 10^6 \text{ m}^3\text{s}^{-1}$ . b) Correlations between the HYCOM model transport and HYCOM proxy transport, for the box transport and jet transport with the percentage of variance shown in brackets. All correlations were significant.

a)	HYCOM (2010-2013)		Proxy		HYCOM (1980-2014)		Proxy	
	$T_{box}$	$T_{jet}$	$T_{box}$	$T_{jet}$	$T_{box}$	$T_{jet}$	$T_{box}$	$T_{jet}$
Transport	$-81 \pm$	$-112 \pm$	$-91 \pm$	$-92 \pm$	$-84 \pm$	$-110 \pm$	$-87 \pm$	$-92 \pm$
Mean & Std (Sv)	53	41	35	30	47	38	34	32
Max (Sv)	-223	-244	-196	-185	-236	-245	-213	-219
Min (Sv)	44	-48	-36	-46	87	-30	-20	-27

b)	$T_{box}$	$T_{jet}$
2010-2013	0.75 (57%)	0.38 (14%)
1980-2014	0.72 (52%)	0.51 (26%)

406 the proxy indicate that transport in HYCOM experiences more variability compared to  
 407 the proxy. The proxies only capture a portion of the transport estimate from the HYCOM  
 408 model, suggesting it also only captures a portion of the model variability. The positive  
 409 minimum transport values for  $T_{box}$  during both time periods also appear to be peculiar,  
 410 suggesting a current reversal during those events (Table 3).

411 Figure 4 shows the correlation between proxy and model transports for each year. The  
 412 correlation per year for  $T_{jet}$  varies greatly from year to year with a significant maximum  
 413 correlation of 0.82 (2014) and an insignificant minimum correlation of 0.00 (2003). In con-  
 414 trast, the correlations for  $T_{box}$  vary much less and are always significant with a maximum  
 415 correlation of 0.88 (1988) and minimum correlation of 0.50 (1994). The box transport  
 416 has higher correlations for most of the 34-year time period except during two single years  
 417 where the jet transport has a higher correlation, 0.78 against 0.70 during 1991 and 0.54  
 418 against 0.50 during 1994. In summary, the results indicate that the proxy is generally  
 419 better suited in HYCOM to estimate the box transport rather than the jet transport.  
 420 Further analysis in this study therefore only focuses on the box transport.

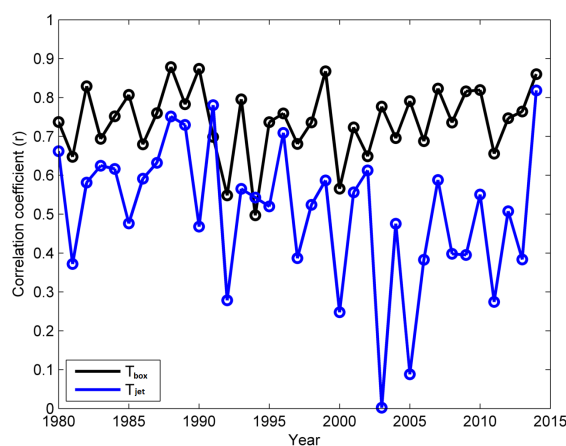


Figure 4: 34-year annual correlations between the box (black) and jet (blue) transport proxies against the box and jet transports extracted from HYCOM.

### 421 3.3 Evaluating the net transport proxy

422 The strengths and weaknesses of the box proxy are further investigated by selecting the  
423 highest and lowest correlated years from the 34-year annual correlations (Figure 4), and  
424 evaluated by plotting the current structure in the model over the respective years (Figures  
425 5 & 6). Investigating the full-depth current structure could emphasize important sub-  
426 surface processes which may not have distinct signatures at the surface and may therefore  
427 be excluded in the transport proxy.

428 Figure 5 shows the surface variability by displaying the eddy kinetic energy and the mean  
429 surface geostrophic flow as represented by the overlaying SSH contours over the 3-year  
430 reference period, and over the highest (1988) and lowest (1994) correlated years of the box  
431 transport proxy. During the reference period the current appears to be stable with low  
432 levels of EKE inshore whereas offshore the flow is more variable with higher levels of EKE.  
433 The flow depicts a similar structure during the lowest correlated year, however, during the  
434 highest correlated year the mean EKE is higher along and downstream of the array with  
435 a relatively stable current structure in comparison to 1994 and 2010-2013. The narrow  
436 spacing of the SSH contours for all three periods indicates a strong gradient inshore and  
437 hence a strong mean geostrophic current, however the wide spacing between the SSH  
438 contours offshore suggests that the variability in the model is confined to the offshore



439 side of the current. It is assumed that high levels of mesoscale variability in the model  
440 could bias the current position and hence the transport estimate, however, based on the  
441 analysis there were approximately five anticyclonic eddies during the highest correlated  
442 year (1988) and  $\sim 7$  anticyclonic eddies during the lowest correlated year which does not  
443 greatly differentiate the accuracy of the proxy for those years.

444 Figure 6 shows the mean cross-track velocity profiles during the reference period (2010-  
445 2013), the highest correlated year (1988) and the lowest correlated year (1994) for each  
446 mooring and the CPIES-pairs. The model cross-track velocity changes direction with  
447 depth, specifically for offshore mooring G and CPIES-pairs P3P4 and P4P5, at the depth  
448 of  $\sim 2000$  m (Figure 6) thereby defining the depth of the Agulhas jet. During the 3-year  
449 reference period the velocity changes direction at moorings B and G ( $\sim 1200$  m and  $\sim 2000$   
450 m respectively) and at sites P3P4 ( $\sim 2000$  m) and P4P5 ( $\sim 300$  m,  $\sim 2000$  m). During 1988  
451 sites F-P4P5 experience a change in direction ( $> \sim 2000$  m). Lastly, during 1994 mooring  
452 G and sites P3P4 and P4P5 exhibit a change in direction ( $> \sim 2000$  m). This shows that  
453 the offshore variability in the model impacts not only the surface variability (Figure 5) but  
454 also the subsurface flow, which would directly impact the accuracy of the box transport  
455 proxy.

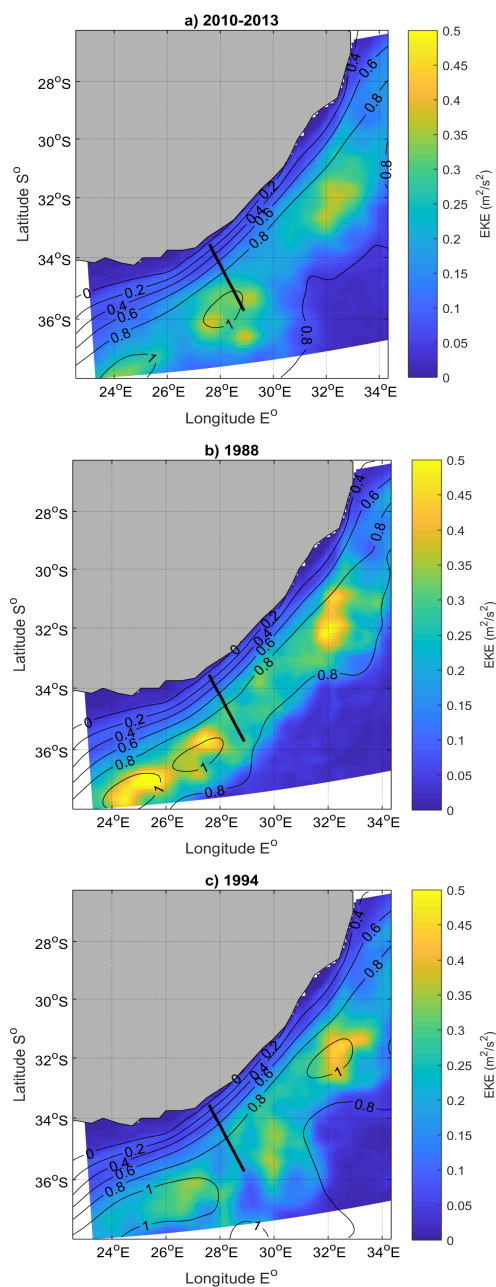


Figure 5: Eddy kinetic energy (EKE in  $\text{m}^2\text{s}^{-2}$ ) and sea surface height (SSH in m) contours during (a) the reference period (2010-2013) (b) the highest (1988) and (c) lowest (1994) correlated years. The black line representing the ACT array.

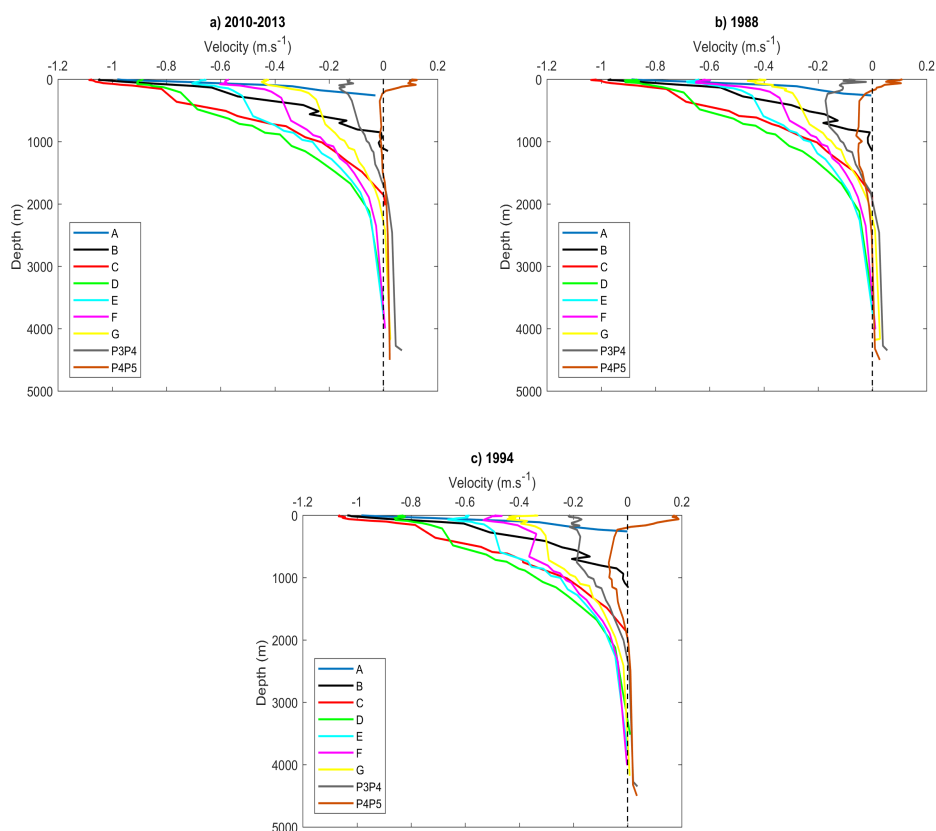


Figure 6: Mean cross-track velocity profiles ( $\text{m s}^{-1}$ ) during (a) the 3-year reference period (2010-2013), (b) during the highest correlated year (1988) and (c) the lowest correlated year (1994). Each colour represents the different moorings (A-G) and CPIES-pairs (P3P4 & P4P5). Negative values indicate southwestward flow.

#### 456 3.4 Investigating the transport variability

457 This section will investigate factors of transport variability in the HYCOM model which  
458 caused the limitations in the HYCOM transport proxy. It was previously shown that  
459 the performance of the linear regression models weakened moving offshore because of the  
460 decrease in correlation between transport per unit distance and SSH slope. Regression  
461 model 8, CPIES-pair P3P4 (RM 8, Figure 7a), captured the least transport variance at  
462 46% and regression model 1, mooring A (RM 1, Figure 7b), explained the most transport  
463 variance at 86%. The differences between the magnitudes of the residual transport events  
464 between RM 1 and RM 8 emphasize a large difference in transport variability between



465 the inshore and offshore mooring locations in HYCOM.

466 According to the methods presented above, a negative SSH slope in HYCOM corresponds  
 467 to a negative (southwest) surface velocity and if the current structure were barotropic, a  
 468 negative (southwest) transport per unit distance estimate and vice versa. As shown in  
 469 regression model 1 (Figure 7b), all the data points are clustered such that the negative  
 470 SSH slope relates to a negative transport per unit distance, in the absence of northeast  
 471 counterflows. Careful analyses of regression model 8 shows that eight of the nine resid-  
 472 ual transport events do violate the proportional relationship between SSH slope and  $T_x$   
 473 (Figure 7a). Some of which have a negative SSH slope relating to a positive transport per  
 474 unit distance where others show a positive SSH slope with negative transport per unit  
 475 distance. Therefore the SSH slope does not always reflect the direction of flow at depth,  
 476 and thus the correct sign for  $T_x$ .

477 Examination of the cross-track velocity structure with depth (Figure 8) shows that there  
 478 is a change in the direction of velocity in the bottom layers at the location of regression  
 479 model 8 (CPIES-pair P3P4). The cross-track flow in the surface layers ( $\sim 0$ -700 m) of the

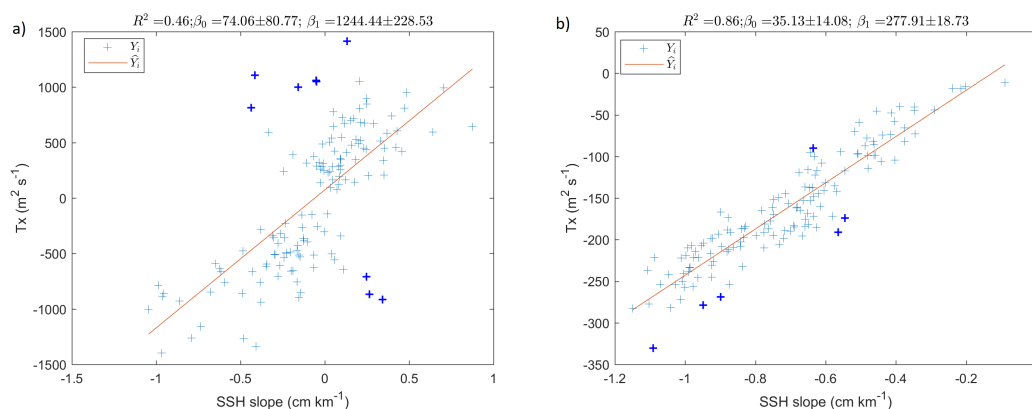


Figure 7: Linear regression models showing the relationship between HYCOM SSH and transport per unit distance ( $T_x$ ) for a) CPIES-pair P3P4 (RM 8); capturing the least transport variance (46%) and b) Mooring A (RM 1); capturing the most transport variance (86%).  $Y_i$  (blue crosses) represent the  $T_x$  values from HYCOM and  $\hat{Y}_i$  (red line) represents the  $T_x$  estimates from the linear regression model. The bold crosses highlight the residual transport events with transport values greater or less than 2 standard deviations of the transport estimate. The coefficient of determination ( $R^2$ ) quantifies the amount of variance explained by the regression model,  $\beta_i$  is the slope coefficient and  $\beta_0$  the intercept with 95% confidence intervals. Note the different scaling on the x & y-axes.

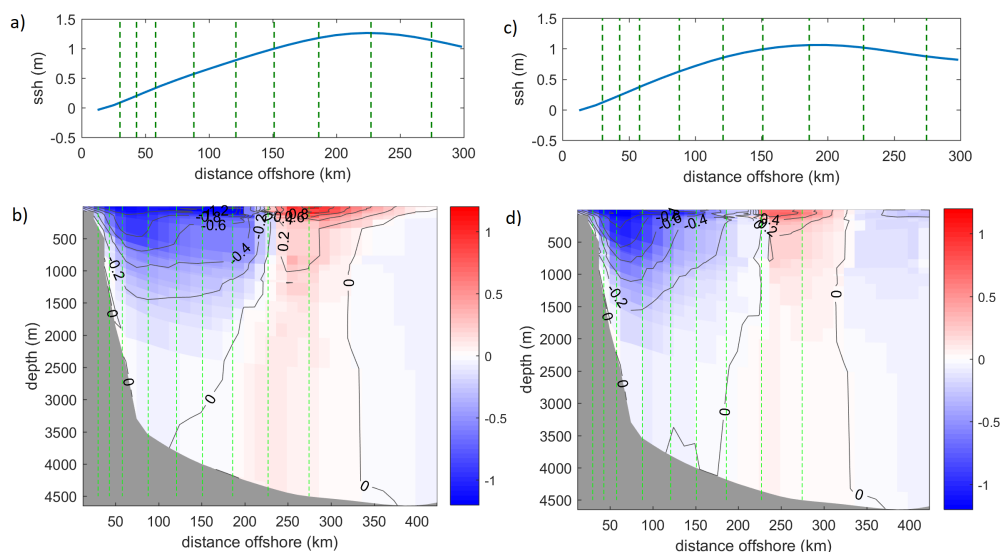


Figure 8: Composite SSH (m) and cross-track velocity structure ( $ms^{-1}$ ) of the residual transport events from a & b) regression model 8 and c & d) regression model 1. Blue shading represents the negative, southwest current direction and red represents the positive, northeast current flow. Contours are every  $0.2 ms^{-1}$ . Dashed vertical lines represents the nine locations of the mooring and CRIES-pairs, the first line representing mooring A and CRIES-pair P4P5 furthest offshore.

480 current is towards southwest, whereas below  $\sim 700$  m the flow is towards the northeast.  
 481 Therefore, the vertically integrated flow ( $T_x$ ) is positive, that is towards the northeast,  
 482 and in the opposite direction implied by the SSH slope. In contrast, at the location of  
 483 mooring A, the composite velocity field is always towards the southwest, that is consistent  
 484 with the SSH slope.

485 The residual investigation (Figures 7 & 8) shows how large outliers decrease the overall  
 486 performance of the linear regression models, by decreasing the percentage of captured  
 487 variance. If these transport events were removed the performance of the linear regres-  
 488 sion models would statistically increase. Removing the outliers larger than  $\pm 2$  standard  
 489 deviations from regression model 8, increases the percentage of captured variance from  
 490 46% to 66%. For model 1, removing outliers increases the captured variance from 86% to  
 491 88%. The improvement is specifically greater for regression model 8 due to the removal of  
 492 the extreme events that violated the directly proportional relationship between SSH slope



493 and transport. Figure 3 shows the increase in the performance of the linear regression  
494 models after the removal of the outlying transport events from all nine regression models.  
495 The increase in variance explained is notable for the regression models corresponding to  
496 the inshore moorings B and C and offshore moorings F, G and CPIES-pairs P3P4 and  
497 P4P5. After the removal of the outlying transport events, the box transport proxy was  
498 re-calculated and its performance compared to the initial proxy. The “improved”  $T_{box}$   
499 proxy captures more variance, 72%, compared to 52% for the original proxy.

### 500 3.5 Sensitivity tests

501 The 34-year Agulhas transport proxy was based on regression models built using only  
502 3 years of HYCOM model data. The statistics in Table 4 and Figure 9 illustrates the  
503 results obtained from building the linear regression models and deriving the transport  
504 proxy using 1, 3, 6, 12, 18 and 34 years of model data. The Taylor diagram (Figure  
505 9) shows the distribution of the results in terms of standard deviation of the transport,  
506 the correlation, and the root-mean-squared error (RMSE) between the proxies and the  
507 HYCOM model transport. We find that the correlation between proxy box transport  
508 and model box transport is not improved by using more model data to build the proxy.  
509 The correlation is 0.72 when using data from 2010-2013, and changes by no more than  
510 0.01 when extending the number of years of model data. Similarly, building the proxy  
511 with one year of model data decreases the correlation by only 0.01 (Figure 9 & Table 4).  
512 The only visible difference was the decrease in standard deviation. It was expected that  
513 the correlation would increase because using more years of model data may capture more  
514 current variability and the RMSE would decrease to correspond to the model transport  
515 estimates.

516 The sensitivity of the box transport proxy was also tested using two arbitrary 3-year peri-  
517 ods. In comparison to the correlation obtained during 2010-2013 the correlation decreased  
518 by 0.02 during 1980-1982 and remained the same during 2000-2002. The results obtained  
519 from calculating the  $T_{box}$  proxy during the maximum (minimum) transport and standard  
520 deviation years in HYCOM showed no improvement or decrease in the skill of the proxy  
521 either.

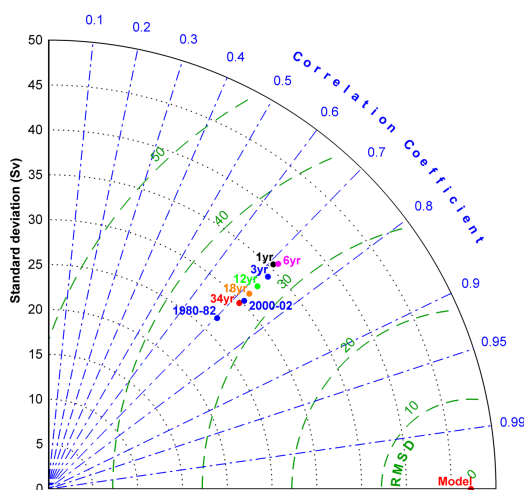


Figure 9: Taylor diagram showing the results of the box transport proxy calculated based on a 1-year linear relationship (black), 3-years (blue), 6-years (magenta), 12-years (green), 18-years (orange), 34-years (red) and during 1980-1982 and 2000-2002 (blue).

Table 4: Transport statistics and correlation results obtained from calculating the net transport proxy over a range of time periods.

Net transport	Transport (Sv)	STD (Sv)	RMSE (Sv)	r
MODEL	-84.32	47.23	0	1.00
1-yr	-87.26	35.47	33.36	0.71
3-yr	-87.21	34.09	32.76	0.72
6-yr	-87.04	35.91	33.04	0.72
12-yr	-86.91	32.51	32.83	0.72
18-yr	-88.71	31.28	32.95	0.72
34-yr	-88.15	29.74	33.14	0.72
1980-1982	-87.86	26.80	34.14	0.70
2000-2002	-94.80	30.31	32.87	0.72

## 522 4 Summary and conclusions

523 The Agulhas Current transport proxies, developed by Beal and Elipot [2016], were based  
 524 on nine linear regression models, each assuming a constant linear relationship from three  
 525 years of observations between *in situ* transport and satellite along-track sea surface gradi-  
 526 ents. Applying constant linear models and assuming a constant vertical current structure,  
 527 the transport proxies were extended using 22-years of along-track satellite data in order to  
 528 yield two 22-year time-series of Agulhas Current transports [Beal and Elipot, 2016]. The  
 529 Agulhas Current transport proxies in the current study replicates the methods used by



530 Beal and Elipot [2016] but applies these using a regional HYCOM model of the Agulhas  
531 Current [Backeberg et al., 2009; 2014]. The HYCOM transport proxies were developed  
532 using nine, three-year linear regression models between model transport and model SSH  
533 slope, and extended using 34-years of the model SSH data from 1980 to 2014.

534 The HYCOM model provided the means to investigate the validity of the assumptions used  
535 to create the proxies, such as the constant relationship between SSH slope and transport  
536 per unit distance at each mooring location and the temporal scale of observations needed  
537 to build a strong linear relationship between transport and SSH slope. Two transport  
538 types, the box transport and the jet transport, were extracted from HYCOM in order  
539 to validate the box transport proxy ( $T_{box}$ ) and the jet transport proxy ( $T_{jet}$ ). The  $T_{box}$   
540 proxy explained a higher percentage of transport variance (57%) during the three-year  
541 reference period (2010-2013), in comparison to the  $T_{jet}$  proxy that only captured 14%  
542 of the variance. Using 34-years of model data (1980-2014), assuming the fixed 3-year  
543 relationship between SSH slope and transport,  $T_{box}$  explained 52% of the variance in  
544 comparison to  $T_{jet}$  that only captured 26%. Results from Beal and Elipot [2016] also  
545 showed that the box transport proxy ( $T_{box}$ ) explained a higher percentage of variance  
546 (61%) during the ACT period than the jet transport proxy ( $T_{jet}$ : 55%).

547 The poorer performance of the  $T_{jet}$  proxy in HYCOM compared to the *in situ*  $T_{jet}$  proxy  
548 of Beal and Elipot [2016] is partly due to various model discrepancies such as the consist-  
549 ent merging of the anticyclonic eddies with the Agulhas Current in the northern region  
550 [Backeberg et al., 2014], in addition to unresolved eddy dissipation in this region [Braby  
551 et al., 2016]. It may also possibly be because it only represents the southwestward flow,  
552 whereas the input sea surface slope reflects the net flow along the array. Therefore, con-  
553 sidering the box transport proxy explains a higher percentage of variance for most of the  
554 34-year period, further analysis on the current structure was based on the  $T_{box}$  proxy only.

555 One of the main assumptions on which the Agulhas transport proxy relies is that the  
556 vertical structure of the current does not change outside the 3-year reference period [Beal  
557 and Elipot, 2016]. There are limitations to the ability of satellite altimeters to detect  
558 sub-surface variability [Robinson, 2004], however, it has been suggested that a strong  
559 relationship between SSH and full-depth transport exists [Beal and Elipot, 2016].



560 The surface structure of the current was investigated in terms of the mean EKE and SSH  
561 contours (Figure 5), which are ideally equivalent to surface geostrophic flow and hence  
562 show the mean horizontal extent of the current [Robinson, 2004]. The vertical variability  
563 was investigated by plotting the mean cross-track velocity profiles (Figure 6). During the  
564 highest correlated year (1988) the current is stable and inshore, whereas during the lowest  
565 correlated year (1994) and during the proxy development period (2010-2013) the current  
566 is meandering and it appears that a large portion of the energy of the current has been  
567 shifted offshore. These results are consistent with Elipot and Beal [2015], who showed that  
568 during the passage of a meander event, a large portion of kinetic energy is extracted from  
569 the flow through the process of barotropic conversion. Results from the analysis of the  
570 vertical profile of the current reveals subsurface counterflows, specifically for the offshore  
571 moorings (G, P3P4 and P4P5) and occasionally for inshore mooring B. An explanation  
572 for the offshore subsurface counter flows may be due to the impinging baroclinic eddies  
573 continuously propagating downstream [Backeberg et al., 2009], which thereby affect the  
574 entire water column by changing the direction of flow at certain depths. This will explain  
575 why the transport proxy fails to capture current reversals, as implied by the positive  
576 minimum transport values in Table 3, because the SSH slope is not reflective of the  
577 subsurface counterflows associated with the impinging baroclinic eddies. The occasional  
578 current reversal for inshore mooring B (43 km offshore, 1264 m depth) may be due to  
579 influence of the simulated Agulhas Undercurrent in HYCOM which flows approximately  
580 40-60 km offshore, 1000-1700 m deep (Figure 8), as opposed to *in situ* estimates of 11-60  
581 km offshore and 1000-2900 m deep [Beal, 2009].

582 The question still remains as to why most of the transport variance was explained in the  
583 year 1988 and the least in 1994? Figure 3 highlighted that the performance of the linear  
584 regression models decreased offshore, such that when the current is in a meandering  
585 state, the  $T_{box}$  proxy fails to accurately estimate the transport. It could be assumed  
586 that using the  $T_{jet}$  proxy would improve the accuracy, however, the performance of the  
587 southwest regression models are only slightly stronger at the offshore end of the array. The  
588 jet transport proxy by Beal and Elipot [2016] was developed to effectively estimate the  
589 transport of the Agulhas Current in the event of a mesoscale meander, which generally  
590 causes the current to manifest as a full-depth, surface intensified, cyclonic circulation



591 out to 150km from the coast with anticyclonic circulation farther offshore [Elipot and  
592 Beal, 2015]. The Agulhas meanders in the HYCOM simulation occur in association with  
593 large anticyclonic eddies predominantly defined to the offshore edge of the current, with a  
594 narrow, southwest stream against the coast [Backeberg et al., 2009] or in some instances  
595 with an anticyclonic eddy across the entire length of the array. The resolution of HYCOM  
596 is able to capture the mesoscale dynamics of eddies [Holton et al., 2017] however, it fails to  
597 resolve the near-coastal features, such as the inshore, surface intensified cyclonic motion  
598 in this simulation. This would require a finer resolution at the coast, in order to reveal  
599 smaller offshore displacements,  $\sim 50$  km, associated with these meander events [Elipot  
600 and Beal, 2015]. The high levels of offshore variability in HYCOM is therefore the main  
601 limiting factor in the performance of both transport proxies.

602 The regression model for CPIES-pair P3P4 (regression model 8) performed the worst, only  
603 explaining 46% of the transport variance (Figure 7a). Evidence from the HYCOM velocity  
604 fields showed that the offshore location of CPIES-pair P3P4 was highly susceptible to the  
605 impinging anticyclonic eddies, which in turn resulted in high levels of variability in the  
606 horizontal and vertical velocity current structure (Figures 7a & 8). The presence of the  
607 anticyclonic eddies would be included in  $T_{box}$ , considering that the eddies produce a strong  
608 surface signature (Figure 5), but the SSH slope might not necessarily be reflective of the  
609 transport beneath the eddy. It has been observed in a layered ocean that, when assuming  
610 geostrophy, the net transport in the uppermost layer ( $\sim 0$ -1000 m) is mainly proportional  
611 to the SSH slope [Andres et al., 2008]. If this was the case, the performance of regression  
612 model 8 would be higher, but the current experiences a baroclinic flow beneath the entire  
613 water column which is not reflective of the SSH slope (Figure 8). As the anticyclonic eddy  
614 crosses the offshore edge of the ACT array, its baroclinic nature in HYCOM effects the  
615 direction of velocity beneath the location of CPIES pair P3P4, which therefore results in  
616 a weak correlation between SSH slope and transport. The impinging anticyclonic eddies  
617 would have a similar influence on the offshore regression models for mooring G and CPIES  
618 pair P4P5 (Figure 8).

619 The regression model for mooring A (regression model 1) performed the best in terms of  
620 the correlation between SSH slope and transport per unit distance (Figure 7b) explaining  
621 86% of the variance. The inshore location of mooring A, 30 km off the coast, experienced



622 low levels of transport variability with a stable southwest current trajectory (Figure 5 &  
623 8) and Figures 6 and 8 illustrate a barotropic current structure in the vicinity of mooring  
624 A with no sub-surface counterflows. The small, sub-surface variability observed inshore of  
625 the array, below 2000 m depth do not necessarily have a direct impact on the SSH signal or  
626 drastically change the volume transport of the water column, however the further offshore,  
627 the closer the interaction of the current with the offshore baroclinic eddies, the weaker  
628 the performance of the regression model.

629 It is important to consider that the Agulhas Current simulation in HYCOM is not com-  
630 pletely realistic, demonstrating much higher levels of mesoscale variability than observed  
631 [Backeberg et al., 2008; 2009]. Rouault and Penven [2011] and Elipot and Beal [2015]  
632 showed that, on average, 1.6 mesoscale meanders pass through the ACT array at 34°S per  
633 year. In the HYCOM simulation an average of 5 anticyclonic eddies passed over the array  
634 per year. A study by Braby et al. [2016] investigating eddy activity in the northern Agul-  
635 has Current using satellite altimetry, showed that both cyclonic and anticyclonic source  
636 eddies dissipate upon approaching the main Agulhas Current. However, the observed  
637 eddy interaction and dissipation process is poorly resolved in many numerical ocean mod-  
638 els [Tsugawa and Hasumi, 2010; Penven et al., 2011; Durgadoo et al., 2013; Backeberg  
639 et al., 2014; Loveday et al., 2014], including the HYCOM model used in this study.

640 The frequently impinging eddies make it difficult to effectively estimate the accurate box  
641 transport of the Agulhas Current in the model since the advection of these eddies have  
642 previously been found to be responsible for large transport fluctuations [Backeberg et al.,  
643 2009]. The transport proxy only includes the transport of the portion of the eddy that  
644 is reflected in the SSH signal across the array, whether it is only the southwestward or  
645 northeastward portion of the eddy or both, and should therefore match the transport  
646 peaks from the model. The transport in the model and proxy may fluctuate accordingly,  
647 however the transport estimates will not necessarily be equivalent, since it also depends  
648 on the strength of the proxy along the ACT array. In other words, the transport proxy  
649 may capture the SSH signal of the eddies along the array, however the correlation of the  
650 regression models decrease offshore, therefore transport estimates inshore would be more  
651 accurate than the transport estimates offshore when the current is in a meandering state.  
652 It was shown that removing the residual transport events violating the proportional rela-



653 tionship between SSH slope and transport improved the proxy performance i.e. increased  
654 the percentage of transport variance explained. Several studies have researched methods  
655 to decrease the levels of EKE in numerical simulations. Backeberg et al. [2009] improved  
656 the representation of the southern Agulhas Current by applying a higher-order momentum  
657 advection scheme, resulting in a well-defined meandering current rather than a continu-  
658 ous stream of eddies. Anderson et al. [2011] found that the use of relative wind forcing  
659 significantly decreased eddy intensities and a study by Renault et al. [2017] focussing on  
660 the current stress feedback between the ocean and atmosphere demonstrated a reduction  
661 of mesoscale activity by deflecting energy from the geostrophic current to the atmosphere,  
662 showing that the indirect current feedback, improved the representation of the Agulhas  
663 Current. Improving the mesoscale variability in the HYCOM model could therefore yield  
664 better results for the transport proxy, specifically for the offshore regression models, in the  
665 future. Furthermore, improving the simulation of coastal, shelf and continental slope fea-  
666 tures, including the Agulhas Undercurrent could decrease the performance of the inshore  
667 regression models. In order to effectively mirror the performance of the *in situ* transport  
668 proxy developed by [Beal and Elipot, 2016] would ideally require a numerical model that  
669 accurately simulates Agulhas meanders and the vertical variability, including an accurate  
670 representation of the Agulhas Undercurrent, which has not yet been achieved in existing  
671 regional configurations.

672 The development of the ACT transport proxy was initially tested using a regional NEMO  
673 configuration in order to evaluate the potential of the altimeter proxy to monitor the  
674 multi-decadal transport of the Agulhas Current [van Sebille et al., 2010]. Using the  
675 numerical model, it was concluded that the correlation between the Agulhas Current  
676 transport and gradient in sea surface height was greater than  $r=0.78$  for any three-year  
677 measuring period, and is therefore an adequate timescale to build an accurate transport  
678 proxy [van Sebille et al., 2010].

679 The HYCOM output in the current study was used to test the validity of the relationship  
680 between transport and SSH slope over a range of time periods. It was hypothesised  
681 that building the linear relationship over longer time periods,  $>3$  years, would increase  
682 the skill of the transport proxy, since the linear relationship would include more current  
683 variability over longer periods of time. The results showed that calculating the transport



684 proxy over longer or shorter time periods did not necessarily improve the performance  
685 of the proxy, thereby suggesting that the current dynamics for any 3-year period in the  
686 model could be very similar, in agreement with the results obtained in van Sebille et al.  
687 [2010], suggesting that the results were consistent despite the model biases. This justifies  
688 that 3-years is a sufficient time-period to develop the satellite-altimeter transport proxy  
689 of the Agulhas Current in HYCOM. Lastly, the study showed that the transport proxy is  
690 sensitive to subsurface variability in the model, suggesting that caution should be taken  
691 regarding the implicit assumption of a fixed vertical current structure. The accuracy of the  
692 transport proxy remains sensitive to model bias and implications therein, suggesting that  
693 these results should be tested rigorously in other model simulations. Sensitivity studies  
694 of this kind, using numerical ocean models, provide useful information into planning *in*  
695 *situ* studies in the future, and understanding the sensitivities and limitations of transport  
696 proxies could further improve long-term monitoring methods in the global ocean.



697 *\*Authors contributions*

698 E.V. conducted the data analyses and wrote up the final paper. B.B provided the HYCOM  
699 model data, supervised the project and provided financial support. J.H. supervised the  
700 project and provided financial support and S.E. assisted with the methodology of the  
701 transport proxy. All authors helped to conceptualize ideas and contributed to writing the  
702 paper.

703 We have no conflicts of interest to disclose.

704 *\*Acknowledgements*

705 This work has been funded by the National Research Foundation of South Africa and  
706 by the bilateral South Africa-Norway SANCOOP SCAMPI project. We would like to  
707 thank the Nansen-Tutu Centre in South Africa and SAEON for providing opportunities  
708 to present the project locally and internationally. We thank the Nansen Environmental  
709 Remote Sensing Centre (NERSC) in Bergen, Norway, for hosting us for a duration of  
710 the project and wish to thank Dr. Knut-Arild Lisæter for his guidance while working at  
711 NERSC. We gratefully acknowledge Professor Lisa Beal, Dr. Shane Elipot and the rest of  
712 the ASCA team from the Rosenstiel School of Marine and Atmospheric Science (RSMAS),  
713 University of Miami, for granting us permission to replicate the Agulhas transport proxy  
714 methods. Shane Elipot was supported by the U.S. National Science Foundation through  
715 the ASCA project, Award OCE-1459543.

716 **References**

- 717 Anderson, L. A., McGillicuddy, D. J., Maltrud, M. E., Lima, I. D., and Doney, S. C.: Im-  
718 pact of eddy-wind interaction on eddy demographics and phytoplankton community  
719 structure in a model of the North Atlantic Ocean, *Dynamics of Atmospheres and*  
720 *Oceans*, 52, 80–94, <https://doi.org/10.1016/j.dynatmoce.2011.01.003>, 2011.
- 721 Andres, M., Park, J.-H., Wimbush, M., X-H, Z., Chang, K., and Ichikawa, H.: Study  
722 of the Kuroshio / Ryukyu Current System Based on Satellite-Altimeter and in situ  
723 Measurements, *Journal of Oceanography*, 64, 937–950, 2008.
- 724 Antonov, J. I. and Levitus, S.: *World ocean atlas 2005. Vol. 2, Salinity*, 2006.
- 725 Backeberg, B. C., Johannessen, J. A., Bertino, L., and Reason, C. J.: The greater Agulhas  
726 Current system: An integrated study of its mesoscale variability, *Journal of Physical*  
727 *Oceanography*, 1, 29–44, 2008.
- 728 Backeberg, B. C., Bertino, L., and Johannessen, J. A.: Evaluating two numerical advec-  
729 tion schemes in HYCOM for eddy-resolving modelling of the Agulhas Current, *Ocean*  
730 *Science*, pp. 173–190, 2009.
- 731 Backeberg, B. C., Penven, P., and Rouault, M.: Impact of intensified Indian Ocean winds  
732 on mesoscale variability in the Agulhas system, *Nature Climate Change*, 2, 608–612,  
733 <https://doi.org/10.1038/nclimate1587>, 2012.
- 734 Backeberg, B. C., Counillon, F., Johannessen, J. a., and Pujol, M. I.: Assimilating along-  
735 track SLA data using the EnOI in an eddy resolving model of the Agulhas system,  
736 *Ocean Dynamics*, pp. 1121–1136, <https://doi.org/10.1007/s10236-014-0717-6>, 2014.
- 737 Beal, L. M.: A Time Series of Agulhas Undercurrent Transport, *Journal of Physical*  
738 *Oceanography*, 39, 2436–2450, <https://doi.org/10.1175/2009JPO4195.1>, 2009.
- 739 Beal, L. M. and Elipot, S.: Broadening not strengthening of the Agulhas Current since  
740 the early 1990s, *Nature Publishing Group*, 540, 570–573, <https://doi.org/10.1038/nature19853>, 2016.
- 741



- 742 Beal, L. M., De Ruijter, W. P. M., Biastoch, A., and Zahn, R.: On the role of the  
743 Agulhas system in ocean circulation and climate., *Nature*, 472, 429–36, [https://doi.org/](https://doi.org/10.1038/nature09983)  
744 10.1038/nature09983, 2011.
- 745 Beal, L. M., Elipot, S., Houk, A., and Leber, G. M.: Capturing the Transport Variability  
746 of a Western Boundary Jet: Results from the Agulhas Current Time-Series Experiment  
747 (ACT)\*, *Journal of Physical Oceanography*, 45, 1302–1324, [https://doi.org/10.1175/](https://doi.org/10.1175/JPO-D-14-0119.1)  
748 JPO-D-14-0119.1, 2015.
- 749 Biastoch, A. and Krauss, W.: The Role of Mesoscale Eddies in the Source Regions of the  
750 Agulhas Current, *Journal of Physical Oceanography*, 29, 2303–2317, 1999.
- 751 Bleck, R.: An oceanic general circulation model framed in hybrid isopycnic-Cartesian  
752 coordinates, 37, 55–88, 2002.
- 753 Braby, L., Backeberg, B. C., Anson, I., Roberts, M. J., Krug, M., and Reason, C. J. C.:  
754 Observed eddy dissipation in the Agulhas Current, *Geophysical Research Letters*, 43,  
755 8143–8150, <https://doi.org/10.1002/2016GL069480>, 2016.
- 756 Cai, W.: Antarctic ozone depletion causes an intensification of the Southern Ocean  
757 super-gyre circulation, *Geophysical Research Letters*, 33, 1–4, [https://doi.org/10.1029/](https://doi.org/10.1029/2005GL024911)  
758 2005GL024911, 2006.
- 759 Chassignet, E. P., Hurlburt, H. E., Martin, O., Halliwell, G. R., Hogan, P. J., Wallcraft,  
760 A. J., Baraille, R., and Bleck, R.: The HYCOM (HYbrid Coordinate Ocean Model) data  
761 assimilative system, 65, 60–83, <https://doi.org/10.1016/j.jmarsys.2005.09.016>, 2007.
- 762 Chelton, D. B., DeSzoeke, R. A., Schlax, M. G., El Naggar, K., and Siwertz, N.: Geograph-  
763 ical Variability of the First Baroclinic Rossby Radius of Deformation, *Journal of Phys-  
764 ical Oceanography*, 28, 433–460, [https://doi.org/10.1175/1520-0485\(1998\)028<0433:](https://doi.org/10.1175/1520-0485(1998)028<0433:GVOTFB>2.0.CO;2)  
765 [GVOTFB>2.0.CO;2](https://doi.org/10.1175/1520-0485(1998)028<0433:GVOTFB>2.0.CO;2), 1998.
- 766 de Ruijter, W. P. M., van Leeuwen, P. J., and Lutjeharms, J. R. E.: Generation and  
767 Evolution of Natal Pulses: Solitary Meanders in the Agulhas Current, *Journal of Phys-  
768 ical Oceanography*, 29, 3043–3055, [https://doi.org/10.1175/1520-0485\(1999\)029<3043:](https://doi.org/10.1175/1520-0485(1999)029<3043:GAEONP>2.0.CO;2)  
769 [GAEONP>2.0.CO;2](https://doi.org/10.1175/1520-0485(1999)029<3043:GAEONP>2.0.CO;2), 1999.



- 770 Dee, D. P., Uppala, S. M., Simmons, A. J., Berrisford, P., Poli, P., Kobayashi, S., Andrae,  
771 U., Balmaseda, M. A., Balsamo, G., Bauer, P., Bechtold, P., Beljaars, A. C. M., Berg,  
772 L. V. D., Bidlot, J., Bormann, N., Delsol, C., Dragani, R., Fuentes, M., Geer, A. J.,  
773 and Dee, D. P.: The ERA-Interim reanalysis : configuration and performance of the  
774 data assimilation system, pp. 553–597, <https://doi.org/10.1002/qj.828>, 2011.
- 775 Dijkstra and de Ruijter, W.: On the Physics of the Agulhas Current : Steady Retroflexion  
776 Regimes, *Journal of Physical Oceanography*, 31, 2971–2985, 2001.
- 777 Durgadoo, J., Loveday, B., Reason, C., Penven, P., and Biastoch, A.: Agulhas Leakage  
778 Predominantly Responds to the Southern Hemisphere Westerlies, *Journal of Physical*  
779 *Oceanography*, 43, 2113–2131, <https://doi.org/10.1175/JPO-D-13-047.1>, 2013.
- 780 Elipot, S. and Beal, L.: Characteristics , Energetics , and Origins of Agulhas Current  
781 Meanders and their Limited Influence on Ring Shedding, *Journal of Physical Oceanog-*  
782 *raphy*, 45, 2294—2314, 2015.
- 783 Elipot, S. and Beal, L. M.: Observed Agulhas Current sensitivity to interannual and  
784 long-term trend atmospheric forcings, *Journal of Climate*, In press, 2018.
- 785 Fu, L.-L., Chelton, D., Le Traon, P.-Y., and Morrow, R.: Eddy Dynamics From Satellite  
786 Altimetry, *Oceanography*, 23, 14–25, <https://doi.org/10.5670/oceanog.2010.02>, 2010.
- 787 George, M. S., Bertino, L., O.M, J., and A, S.: Validation of a hybrid coordinate  
788 ocean model for the Indian Ocean, *Journal of Operational Oceanography*, 3, 25–38,  
789 <https://doi.org/10.1080/1755876X.2010.11020115>, 2010.
- 790 Gordon, A. L.: Oceanography: The brawniest retroflexion, *Nature*, 421, 904–905,  
791 <https://doi.org/10.1038/421904a>, 2003.
- 792 Gordon, A. L., Lutjeharms, J. R., and Gründlingh, M. L.: Stratification and circulation at  
793 the Agulhas Retroflexion, *Deep Sea Research Part A. Oceanographic Research Papers*,  
794 34, 565–599, [https://doi.org/10.1016/0198-0149\(87\)90006-9](https://doi.org/10.1016/0198-0149(87)90006-9), 1987.
- 795 Hermes, J. C., Reason, C., and Lutjeharms, J.: Modeling the Variability of the Greater  
796 Agulhas Current System, *Journal of climate*, 20, 3131–3146, <https://doi.org/10.1175/JCLI4154.1>, 2007.



- 798 Holton, L., Deshayes, J., Backeberg, B., Loveday, B., Hermes, J., and Reason, C.: Spatio-  
799 temporal characteristics of Agulhas leakage: a model inter-comparison study, *Climate*  
800 *dynamics*, 48, 2107–2121, 2017.
- 801 Imawaki, S., Uchida, H., Ichikawa, H., and Fukasawa, M.: Satellite altimeter monitoring  
802 the Kuroshio transport south of Japan, *Geophysical Research Letters*, 28, 17–20, 2001.
- 803 Loveday, B. R., Durgadoo, J. V., Reason, C. J., Biastoch, A., and Penven, P.: Decoupling  
804 of the Agulhas leakage from the Agulhas Current, *Journal of Physical Oceanography*,  
805 44, 1776–1797, <https://doi.org/10.1175/JPO-D-13-093.1>, 2014.
- 806 Lutjeharms, J. R. E.: *The Agulhas Current*, 2006.
- 807 Maul, G. A., Mayer, D. A., and Bushnell, M.: Statistical relationships between local sea  
808 level and weather with Florida-Bahamas cable and Pegasus measurements of Florida  
809 Current volume transport, *Journal of Geophysical Research*, 95, 3287–3296, 1990.
- 810 Penven, P., Herbette, S., and Rouault, M.: Ocean Modelling in the Agulhas Current  
811 System, in: *Nansen-Tutu Conference Proceedings*, pp. 17–21, [https://doi.org/10.1017/](https://doi.org/10.1017/CBO9781107415324.004)  
812 [CBO9781107415324.004](https://doi.org/10.1017/CBO9781107415324.004), 2011.
- 813 Reason, C. J. C.: Subtropical Indian Ocean SST dipole events and southern African  
814 rainfall, *Geophysical Research Letters*, 28, 2225–2227, 2001.
- 815 Renault, L., McWilliams, J. C., Penven, P., Renault, L., McWilliams, J. C., and Pen-  
816 ven, P.: Modulation of the Agulhas Current Retroflexion and Leakage by Oceanic  
817 Current Interaction with the Atmosphere in Coupled Simulations, *Journal of Physical*  
818 *Oceanography*, 47, 2077–2100, <https://doi.org/10.1175/JPO-D-16-0168.1>, 2017.
- 819 Robinson, I. S.: *Measuring the oceans from space: the principles and methods of satellite*  
820 *oceanography*, Springer Science & Business Media, 2004.
- 821 Rouault, M. and Lutjeharms, J.: Estimation of sea-surface temperature around southern  
822 Africa from satellite-derived microwave observations., *South African journal of science*,  
823 99, 489–493, 2003.
- 824 Rouault, M., White, S. A., Reason, C. J. C., Lutjeharms, J. R. E., and Jobard, I.:  
825 *Ocean Atmospheric Interaction in the Agulhas Current Region and a South African*



826 Extreme Weather Event, *Weather and Forecasting*, 17, 655–669, [https://doi.org/10.1175/1520-0434\(2002\)017<0655:OAIITA>2.0.CO;2](https://doi.org/10.1175/1520-0434(2002)017<0655:OAIITA>2.0.CO;2), 2002.

828 Rouault, M. J. and Penven, P.: New perspectives on Natal Pulses from satellite ob-  
829 servations, *Journal of Geophysical Research: Oceans*, 116, 1–14, <https://doi.org/10.1029/2010JC006866>, 2011.

831 Rouault, M. J., Mouche, A., Collard, F., Johannessen, J. A., and Chapron, B.: Mapping  
832 the Agulhas Current from space : An assessment of ASAR surface current velocities,  
833 *Journal of Geophysical Research*, 115, 1–14, <https://doi.org/10.1029/2009JC006050>,  
834 2010.

835 Smith, L., , Boudra, D., and R, B.: A Wind-Driven Isopycnic Coordinate Model of the  
836 North and Equatorial Atlantic Ocean 2 . The Atlantic Basin Experiments, *Journal of*  
837 *Geophysical Research*, 95, 105–128, 1990.

838 Sprintall, J. and Revelard, A.: The Indonesian Throughflow response to Indo-Pacific  
839 climate variability, *Journal of Geophysical Research: Oceans*, 119, 1161–1175,  
840 <https://doi.org/10.1002/2013JC009533>.Received, 2014.

841 Tsugawa, M. and Hasumi, H.: Generation and Growth Mechanism of the Natal  
842 Pulse, *Journal of Physical Oceanography*, 40, 1597–1612, <https://doi.org/10.1175/2010JPO4347.1>, 2010.

844 Uppala, S. M., Kallberg, P. W., Simmons, A. J., Andrae, U., Bechtold, V. D. C., Fiorino,  
845 M., Gibson, J. K., Haseler, J., Hernandez, A., Kelly, G. A., Li, X., Onogi, K., Saarinen,  
846 S., Sokka, N., Allan, R. P., Andersson, E., Arpe, K., Balmaseda, M. A., Beljaars, A.  
847 C. M., Berg, L. V. D., Bidlot, J., Bormann, N., Caires, S., Chevallier, F., Dethof,  
848 A., Dragosavac, M., Fisher, M., Fuentes, M., Hagemann, S., Holm, E., Hoskins, B. J.,  
849 Isaksen, L., Janssen, P. A. E. M., Jenne, R., McNally, A. P., Mahfouf, J., Morcrette,  
850 J., Rayner, N. A., Saunders, R. W., Simon, P., Sterl, A., Trenberth, K. E., Untch, A.,  
851 Vasiljevic, D., Viterbo, P., and Woollen, J.: The ERA-40 re-analysis, *Quarterly Journal*  
852 *of the Royal Meteorological Society*, 131, 2961–3012, <https://doi.org/10.1256/qj.04.176>,  
853 2005.



854 van Sebille, E., Beal, L. M., and Biastoch, A.: Sea surface slope as a proxy for  
855 Agulhas Current strength, *Geophysical Research Letters*, 37, 2–5, [https://doi.org/](https://doi.org/10.1029/2010GL042847)  
856 10.1029/2010GL042847, 2010.

857 Yan, X. M. and Sun, C.: An altimetric transport index for Kuroshio inflow northeast  
858 of Taiwan Island, *Science China Earth Sciences*, 58, 697–706, [https://doi.org/10.1007/](https://doi.org/10.1007/s11430-014-5024-z)  
859 s11430-014-5024-z, 2015.

860 Yang, H., Lohmann, G., Wei, W., Dima, M., Ionita, M., and Liu, J.: Intensification  
861 and poleward shift of subtropical western boundary currents in a warming climate,  
862 *Journal of Geophysical Research: Oceans*, 121, 4928–4945, [https://doi.org/10.1002/](https://doi.org/10.1002/2015JC010796)  
863 2015JC010796, 2016.

864 Zhu, X. H., Ichikawa, H., Ichikawa, K., and Takeuchi, K.: Volume transport variability  
865 southeast of Okinawa Island estimated from satellite altimeter data, *Journal of Ocean-*  
866 *ography*, 60, 953–962, <https://doi.org/10.1007/s10872-005-0004-8>, 2004.